Use of multicorrelator techniques for interference detection

Christophe Macabiau, Olivier Julien, Eric Chatre

Use of Multicorrelator Techniques for Interference Detection

Christophe MACABIAU, *ENAC*
Olivier JULIEN, *ENAC*
Eric CHATRE, *STNA*

BIOGRAPHY

Christophe Macabiau graduated as an electronics engineer in 1992 from the ENAC (Ecole Nationale de l'Aviation Civile) in Toulouse, France. Since 1994, he has been working on the application of satellite navigation techniques to civil aviation. He received his Ph.D. in 1997 and has been in charge of the signal processing lab of the ENAC since 2000.

Olivier Julien will graduate in 2001 as an electronics engineer from the Ecole Nationale de l'Aviation Civile (ENAC) in Toulouse, France.

Eric Chatre graduated as an electronics engineer in 1992 from the ENAC (Ecole Nationale de l'Aviation Civile), Toulouse, France. Since 1994, he has been working with the Service Technique de la Navigation Aérienne (STNA) in Toulouse on implementation of satellite navigation in civil aviation. He is involved in the development of EGNOS and in the definition phase of Galileo. He is also participating in GNSS standardization activities in ICAO GNSSP and EUROCAE, RTCA forums.

ABSTRACT

The interference is among the most feared events in civil aviation use of GNSS. A large number of techniques were designed to alleviate the sensitivity of modern receivers to this perturbation. Most of these techniques are either based on spatial discrimination like adaptive antennas, on spectral selectivity such as notch filters or on amplitude detection. The advent of multicorrelator receivers widens the range of methods that can be considered to tackle this problem. In particular, this enables the characterization of interference effects on the tracking loops through the analysis of the shape of the correlation peak.

The aim of this paper is to present the observed effect of CW and FM interference on the correlation peak with a real receiver, to compare this result with theoretical expressions and characterize the resulting pseudorange and position errors.

The paper starts with the theoretical derivation of the effect of CW interference on the code and phase tracking loops I and Q samples for a typical receiver. Based on these results, specification of a test equipment is derived allowing real data collection. Results of CW interference tests are described for different test configurations.

Correlation peak and pseudorange error measurements are collected for different CW interferer frequencies and power levels. These observations were used to validate the theoretical derivations mentioned above, therefore demonstrating the feasibility of interference detection with multicorrelator techniques. These tests were further extended to FM type interference with different bandwidths and power levels and yielded similar results.

End-to-end testing is finally carried out on a standard receiver to determine the impact of the interference on a multi-channel receiver, showing that the position output can be significantly disturbed if the interference is not detected.

I. INTRODUCTION

Several types of perturbations can affect the signal processed by a GPS receiver. These perturbations are thermal noise, atmospheric disturbances, multipath and interference. Interference remains the most feared perturbation for civil aviation users because it can affect several tracking channels at a time during a long period.

A wide number of techniques were designed to increase the robustness of the processing operations carried out by the GPS receiver [Ward, 1996], [Spilker and Natali, 1996].

The first critical element is the antenna, which can be designed as an adaptive antenna array that either provides additional antenna gain in the direction of each satellite through beamforming, or nulls out interference signals coming from point sources.

Next, front-end filters are designed in RF or IF to reduce out-of-band interference. Adaptive frequency notch filters can also be implemented to attenuate in-band narrow-band interference [Przyjemski et al., 1993]. Then, the use of an ADC mapping on a large number of bits/sample and proper AGC can reduce non linear signal suppression effects. Adaptive ADC can also reduce constant envelope interference effects.

Finally, reducing the loops bandwidth can reduce their sensitivity to a large class of interferers. Similarly, this can also be achieved using aiding from other sensors such as the INS [Bye et al., 1998].

II. EFFECT OF CW TONE ON I AND Q SAMPLES

Let us consider the case where the signal entering the tracking loops is only affected by a pure CW sinusoidal carrier plus noise. We assume the signal is not affected by multipath.

The expression of that incoming signal is therefore:

$$V(k) = A \times D(kT_s - \tau)C(kT_s - \tau)\cos\left(2\pi f_I kT_s - \theta\right) + A_J \times \cos\left(2\pi\left(f_I + \Delta f\right)kT_s - \theta_J\right) + n(k)$$

where

- A is the amplitude of the line-of-sight signal
- D and C are the P/NRZ/L waveforms associated to the navigation message and to the C/A code
- f_I is the final intermediate frequency
- T_s is the sampling period and $F_s=1/T_s$ is the sampling frequency
- θ is the carrier phase shift of the line-of-sight signal
- τ is the group propagation delay of the line-of-sight signal
- A_J is the amplitude of the CW jammer
- Δf is the frequency offset of the transmitted jammer signal with respect to L1
- θ_J is the time-dependent phase shift of the jammer
- n is the noise superimposed to the signal

Note that the amplitude values A and A_J are dependent upon the initial amplitude of the GPS signal and jammer at the output of the antenna, but also on the rejection provided by the RF/IF filters in conjonction with the performance of the AGC/ADC.

The signal on the I and Q branches of the phase tracking loop have the following expression:

$$\begin{cases} V_I(k) = V(k) \times \cos\left(2\pi f_I kT_s - \hat{\theta}\right) \times C(kT_s - \hat{\tau}) \\ V_Q(k) = V(k) \times \sin\left(2\pi f_I kT_s - \hat{\theta}\right) \times C(kT_s - \hat{\tau}) \end{cases}$$

Assuming the high frequency terms are removed after integration, condition which is fulfilled even if the receiver is tracking the jammer, the output of the I&D filters is:

$$\begin{cases} I(n) = \dfrac{A}{2} D(n) R(\varepsilon_D) \cos\varepsilon_P + \dfrac{A_J}{2} \displaystyle\sum_{k=(n-1)M}^{nM-1} \cos\left(2\pi\Delta f kT_s - \theta_J + \hat{\theta}\right) C(kT_s - \hat{\tau}) + n_I(n) \\ Q(n) = \dfrac{A}{2} D(n) R(\varepsilon_D) \sin\varepsilon_P - \dfrac{A_J}{2} \displaystyle\sum_{k=(n-1)M}^{nM-1} \sin\left(2\pi\Delta f kT_s - \theta_J + \hat{\theta}\right) C(kT_s - \hat{\tau}) + n_Q(n) \end{cases}$$

where

- n is the index of the time series at the output of the I&D filters
- $\varepsilon_P = \theta - \hat{\theta}$ is the carrier phase tracking error
- $\varepsilon_D = \tau - \hat{\tau}$ is the code tracking error
- M is the number of samples accumulated by the I&D filters
- n_I and n_Q are the signals resulting from the integration of the noise samples.

The two additional terms in the I and Q samples delivered by the I&D filters are in fact the result of the correlation between the local generated code and the additive CW tone. These two terms are

$$\begin{cases} R_I(\hat{\tau}, n) = \displaystyle\sum_{k=(n-1)M}^{nM-1} \cos\left(2\pi\Delta f kT_s - \theta_J + \hat{\theta}\right) C(kT_s - \hat{\tau}) \\ R_Q(\hat{\tau}, n) = \displaystyle\sum_{k=(n-1)M}^{nM-1} \sin\left(2\pi\Delta f kT_s - \theta_J + \hat{\theta}\right) C(kT_s - \hat{\tau}) \end{cases}$$

Denoting $\Delta\theta = \theta_J - \hat{\theta}$ the phase difference, we can re-write these expressions as:

$$\begin{cases} R_I(\hat{\tau}, n) = \displaystyle\sum_{k=-\infty}^{+\infty} c(k) C(k - \hat{\tau}/T_s) \\ R_Q(\hat{\tau}, n) = \displaystyle\sum_{k=-\infty}^{+\infty} s(k) C(k - \hat{\tau}/T_s) \end{cases}$$

where

- $c(k) = \cos\left(2\pi\Delta f kT_s - \Delta\theta\right) \times \mathrm{rect}\left(\dfrac{kT_s - T_n}{T_D}\right)$
- $s(k) = \sin\left(2\pi\Delta f kT_s - \Delta\theta\right) \times \mathrm{rect}\left(\dfrac{kT_s - T_n}{T_D}\right)$
- *rect(x)* is the rectangular window function
- $T_n = (n - 0.5)MT_s$ is the centre of the current summation window.

We can re-write these expressions using the discrete signal Fourier transform:

$$\begin{cases} R_I(f,n) = c(f)C_d(f) \\ R_Q(f,n) = s(f)C_d(f) \end{cases}$$

where $C_d(f)$ is the discrete signal Fourier transform of $C(k)$.

Assuming the Shannon condition is fulfilled, the discrete signal Fourier transforms of the windowed cosine and sine functions $c(k)$ and $s(k)$ have the following expressions for $f \in \left[-\frac{F_s}{2};\frac{F_s}{2}\right[$:

$$c(f) = \left[\frac{1}{2}\delta(f-\Delta f)e^{-i\Delta\theta} + \frac{1}{2}\delta(f+\Delta f)e^{i\Delta\theta}\right] * \left[T_D e^{-i\pi f T_n}\frac{\sin \pi f T_D}{\pi f T_D}\right]$$

$$s(f) = \left[\frac{1}{2i}\delta(f-\Delta f)e^{-i\Delta\theta} - \frac{1}{2i}\delta(f+\Delta f)e^{i\Delta\theta}\right] * \left[T_D e^{-i\pi f T_n}\frac{\sin \pi f T_D}{\pi f T_D}\right]$$

where T_D=20 ms is the I&D integration duration.

As illustrated in figure 1, we can see that $c(f)$ and $s(f)$ are composed of two *sinc* with a main lobe of width *[-50 Hz; +50 Hz]* located in -Δf and +Δf.

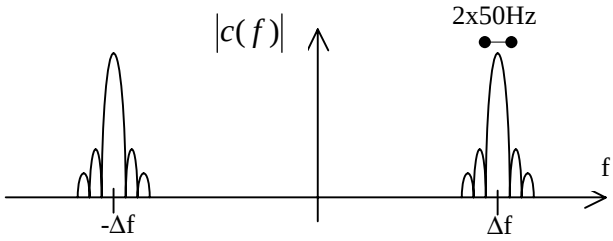

Figure 1: *Magnitude of Fourier transform of windowed CW jammer*

Similarly, the discrete signal Fourier transform of C_d is the product of the Fourier transform of the P/NRZ/L waveform with the Fourier transform of the C/A Gold code. This discrete signal Fourier transform can be expressed as:

$$C_d(f) = \sum_{k=-\infty}^{+\infty}\frac{1}{1023}\frac{\sin\frac{\pi k}{1023}}{\frac{\pi k}{1023}}C_0(k)\delta(f-kf_R)$$

for $f \in \left[-\frac{F_s}{2};\frac{F_s}{2}\right[$, where C_0 is the discrete Fourier transform of the tracked C/A Gold code. This discrete Fourier transform C_0 is periodic with period 1023.

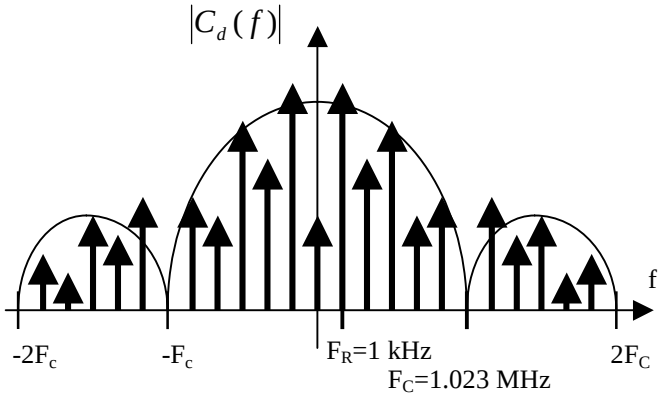

Figure 2: *Magnitude of Fourier transform of P/NRZ/L waveform representing the C/A code.*

As illustrated in figure 2, $C_d(f)$ is a pure line spectrum. Each dirac line has a weight which is the product of the *sinc* weighting function originating from the P/NRZ/L materialization of the code, with the individual weight of the line in the C/A code discrete Fourier transform.

We can simplify this expression into

$$C_d(f) = \sum_{k=-\infty}^{+\infty} C_{\text{sinc}}(k)\delta(f-kf_R)$$

where $C_{\text{sinc}}(k) = \frac{1}{1023}\frac{\sin\frac{\pi k}{1023}}{\frac{\pi k}{1023}}C_0(k)$.

We can simplify the expression of $R_I(f,n)$ and $R_Q(f,n)$ by considering that only the C/A code lines of $C_d(f)$ that fall inside the two *sinc* main lobes of $c(f)$ and $s(f)$ do yield a significant cross-correlation output. In that case, $R_I(f,n)$ can be expressed as:

$$R_I(f,n) = \left[\frac{T_D}{2}e^{-i\pi(f-\Delta f)T_n}\frac{\sin\pi(f-\Delta f)T_D}{\pi(f-\Delta f)T_D}e^{-i\Delta\theta}\right] \times C_{\text{sinc}}(k_0)\delta(f-k_0 f_R) + \left[\frac{T_D}{2}e^{-i\pi(f+\Delta f)T_n}\frac{\sin\pi(f+\Delta f)T_D}{\pi(f+\Delta f)T_D}e^{i\Delta\theta}\right] \times C_{\text{sinc}}(-k_0)\delta(f+k_0 f_R)$$

where k_0 is the index of the C/A code spectrum line such that $k_0 f_R \in \left[\Delta f - \frac{f_D}{2};\Delta f + \frac{f_D}{2}\right]$.

Simplifying these expressions, we get:

$$R_I(f,n) = T_D e^{-i\pi f T_n} \times$$
$$\left[\begin{array}{l} \frac{1}{2} e^{i\pi\Delta f T_n} \frac{\sin\pi(f-\Delta f)T_D}{\pi(f-\Delta f)T_D} e^{-i\Delta\theta} C_{\text{sinc}}(k_0)\delta(f-k_0 f_R) \\ + \frac{1}{2} e^{-i\pi\Delta f T_n} \frac{\sin\pi(f+\Delta f)T_D}{\pi(f+\Delta f)T_D} e^{i\Delta\theta} C_{\text{sinc}}(-k_0)\delta(f+k_0 f_R) \end{array} \right]$$

Denoting $\delta f = k_0 f_R - \Delta f$ and $C_0(k_0) = |C_0(k_0)| e^{i\varphi(k_0)}$, we have

$$R_I(f,n) = T_D e^{-i\pi f T_n} \times \frac{\sin\pi\delta f T_D}{\pi\delta f T_D}$$
$$\times \left[\begin{array}{l} \frac{1}{2} e^{i\pi\Delta f T_n} e^{-i\Delta\theta} |C_{\text{sinc}}(k_0)| e^{i\varphi(k_0)} \delta(f-k_0 f_R) \\ + \frac{1}{2} e^{-i\pi\Delta f T_n} e^{i\Delta\theta} |C_{\text{sinc}}(k_0)| e^{-i\varphi(k_0)} \delta(f+k_0 f_R) \end{array} \right]$$

We can then convert back this expression in the frequency domain into the following expression in the time domain:

$$R_I(\hat{\tau},n) = T_D \times |C_{\text{sinc}}(k_0)| \times \frac{\sin\pi\delta f T_D}{\pi\delta f T_D}$$
$$\cos\left(2\pi k_0 f_R \left(\hat{\tau} - \frac{T_n}{2} \right) + 2\pi\Delta f \frac{T_n}{2} - \Delta\theta + \varphi(k_0) \right)$$

Similarly, it can be shown that $R_Q(\hat{\tau},n)$ can be expressed as:

$$R_Q(\hat{\tau},n) = T_D \times |C_{\text{sinc}}(k_0)| \times \frac{\sin\pi\delta f T_D}{\pi\delta f T_D}$$
$$\sin\left(2\pi k_0 f_R \left(\hat{\tau} - \frac{T_n}{2} \right) + 2\pi\Delta f \frac{T_n}{2} - \Delta\theta + \varphi(k_0) \right)$$

Denoting $\varphi(n) = 2\pi(\Delta f - k_0 f_R)\frac{T_n}{2} - \Delta\theta + \varphi(k_0)$, the final expression of the I and Q samples is

$$\left\{ \begin{array}{l} I(n) = \frac{A}{2} D(n) R(\varepsilon_D) \cos\varepsilon_P \\ + \frac{A_J}{2} T_D |C_{\text{sinc}}(k_0)| \frac{\sin\pi\delta f T_D}{\pi\delta f T_D} \cos(2\pi k_0 f_R \hat{\tau} + \varphi(n)) \\ + n_I(n) \\ Q(n) = \frac{A}{2} D(n) R(\varepsilon_D) \sin\varepsilon_P \\ - \frac{A_J}{2} T_D |C_{\text{sinc}}(k_0)| \frac{\sin\pi\delta f T_D}{\pi\delta f T_D} \sin(2\pi k_0 f_R \hat{\tau} + \varphi(n)) \\ + n_Q(n) \end{array} \right.$$

Therefore, as we can see from these final expressions, the I and Q correlator outputs of the tracking loops are disturbed by additive cosine and sine terms. The influence of the jammer highly depends on the relative amplitude of these additive oscillations with respect to the amplitude of the received line-of-sight code correlation. This relative amplitude depends

- on the direct ratio of the received jammer power with respect to the received GPS signal power
- on the 50 Hz *sinc* of the frequency offset of the received jammer with respect to the received signal frequency
- on the weight of the P/NRZ/L C/A code line which is being hit by the jammer

III. TEST EQUIPMENT

To test the validity of the theoretical development presented in section II, and to determine a way to detect the presence of interfering signals in the tracking loops, we have decided to conduct some experiments with an interference generator, a RF GPS signal generator and a multicorrelator receiver.

Classical receivers offer several tracking channels, each of them being driven by two pairs of correlator outputs. A multicorrelator receiver provides values of the correlation of the incoming signal with several delayed replicas of the same local code in a single tracking channel. In that case, we get simultaneously several I and Q samples for each relative delay *d* of each replica with respect to punctual.

For the experiment described here, we have used a Novatel Millenium receiver whose software has been modified so as to provide 2 tracking channels, one of them just providing 2 correlator outputs on I and Q, and the second one providing 46 correlator outputs both on I and Q for interference analysis. The desired offset of the 46 correlators with respect to punctual was designed by setting a compromise between the resolution and the maximum interfering signal frequency that can be identified. We have decided to place the 46 correlators with a step of 0.25 chip from –5.9 chips to 5.1 chips from punctual. This provides an analysis window of 11 chips, and enables an unambiguous detection of interfering signals up to 2 MHz around L1.

The operations performed in each correlation channel are illustrated in figure 3.

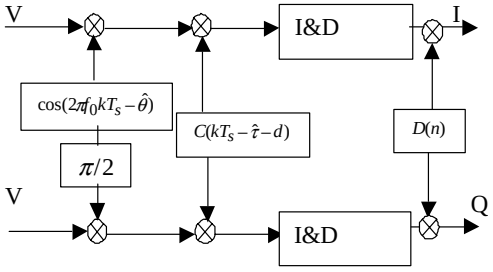

Figure 3: *Architecture of one correlator output.*

We can deduce the expression of the correlator outputs in presence of a CW jammer from the final expressions obtained in section II.

$$\begin{cases} I(n) = \dfrac{A}{2} R(\varepsilon_D - d)\cos\varepsilon_P \\ + \dfrac{A_J}{2} T_D D(n) \left|C_{\text{sinc}}(k_0)\right| \dfrac{\sin \pi\delta f T_D}{\pi\delta f T_D} \cos\left(2\pi k_0 f_R d + \psi(n)\right) \\ + n_I(n) \\ Q(n) = \dfrac{A}{2} R(\varepsilon_D - d)\sin\varepsilon_P \\ - \dfrac{A_J}{2} T_D D(n) \left|C_{\text{sinc}}(k_0)\right| \dfrac{\sin \pi\delta f T_D}{\pi\delta f T_D} \sin\left(2\pi k_0 f_R d + \psi(n)\right) \\ + n_Q(n) \end{cases}$$

where $\psi(n) = 2\pi k_0 f_R \hat{\tau} - \varphi(n)$.

The interference generator is a Rohde and Schwarz signal generator SME03. It is used in this experiment to generate a CW tone and an FM modulated carrier. The uncertainty in the output power level was determined to be ± 1 dB W for power levels around –100 dB W.

For this experiment, the GPS signals used were generated by a GSS RF GPS signal generator. The power level of each of the GPS signals at the output of the GSS generator was set to be fixed throughout the scenario at a level of –140 dBW. This yields a average C/N_0 of 48.5 dB Hz as estimated by the Novatel receiver.

In order to compare the characteristics of the jammer and the received GPS signal, both generators are connected to a spectrum analyzer. The GPS signal fed to the spectrum analyzer is grabbed from the back output of the GSS RF signal generator that is significantly amplified.

The equipment set-up is presented in figure 4.

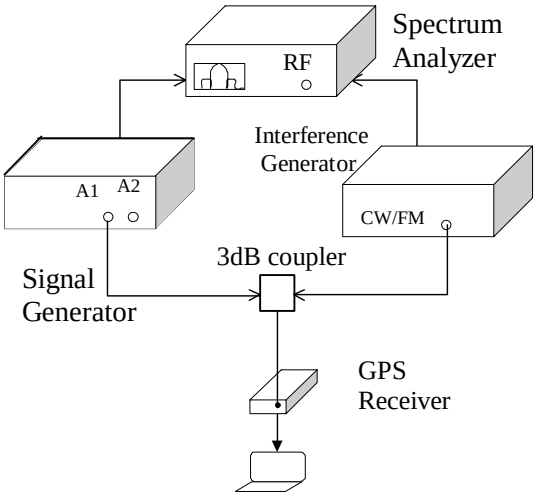

Figure 4: *Test equipment set-up.*

In this set-up, the output of the RF GPS signal generator is added to the output of the interference generator with a 3dB coupler. The power of each of the GPS signals entering the receiver is therefore –143 dBW.

Figure 5 presents an example of spectrum for a specific test. In this figure, we can distinguish between two lines of the PRN 6 C/A code and the jammer tone. The display grid is 200 Hz x 10 dB. The lines appear like *sinc* because the resolution bandwidth was set to 100 Hz.

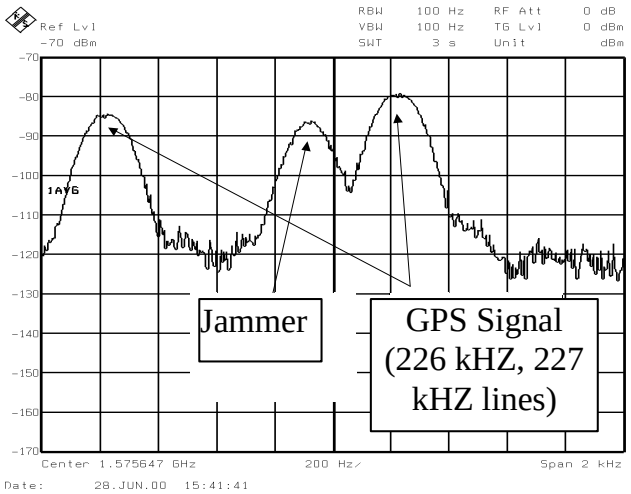

Figure 5: *Snapshot showing the spectrum of the signal fed to the receiver.*

IV. OBSERVED EFFECT OF CW INTERFERENCE

The first tests that were conducted aimed at verifying the theoretical developments presented in section II of this paper. To do that, we decided to analyze the effects of a jammer on two distinct lines of a C/A code. We first chose to jam the highest line of PRN 6 C/A code, and then an average line.

The highest line of PRN 6 C/A code has a frequency of 227 kHz and an individual relative power of –21.29 dBW with respect to the total power of the C/A code.

To jam that code line, we configured the GPS signal generator with a scenario in which the Doppler of the received PRN 6 signal crosses 0. The CW signal generator was set to deliver a tone at L1+227 kHz with an output power of -132 dBW. Considering the 3dB coupler used to add the GPS signals and the jammer, the power of the interferer at the input of the receiver is therefore –135 dBW, and the power of the GPS signal is –143 dBW.

Figure 6 shows a superposition of several correlation peaks as seen on the I channel when no jamming signal is applied. In that case, the correlation peak is only affected by noise, which has a fairly low level as C/N_0 = 49 dHz as seen by the receiver. The shape of the feet of the observed triangle is exactly due to the autocorrelation sidelobes of PRN 6.

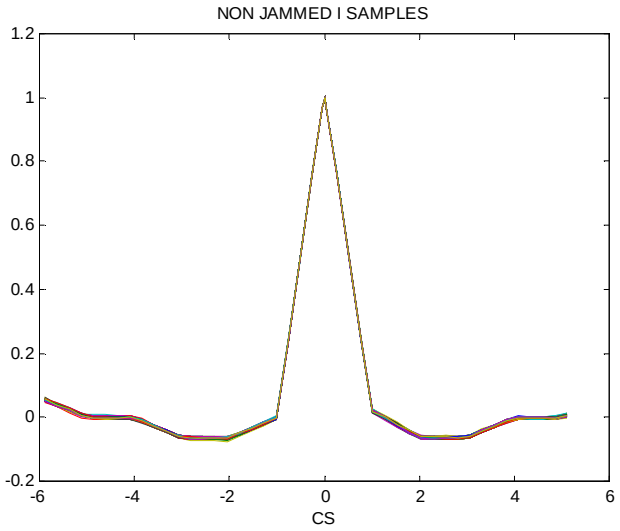

Figure 6: *Observed correlation peak in the absence of jammer.*

Figure 7 shows the evolution of the C/N_0 as computed by the receiver throughout the test. As we can see, in the beginning of the test, when no jammer is present, the C/N0 is equal to 49 dB Hz.

Throughout the experiment, the tracking channel never experienced loss of lock. During the first minute after the jammer is turned on, the estimated C/N_0 oscillates between 45.5 dB Hz and 49.5 dB Hz. After this transient period, the C/N_0 estimate is stable at 48.4 dB Hz, which is 0.6 dB below its initial value.

This steady value of the estimated C/N_0 can be predicted from the values used by the receiver to compute that estimate. The noise power density N_0 is estimated from the detected distribution of the samples in the ADC. The signal power C is extracted from the sum of the squared I and Q punctual samples in the PLL. That type of predicted effect on the estimated C/N_0 for Gaussian interference is presented in [Betz, 2000].

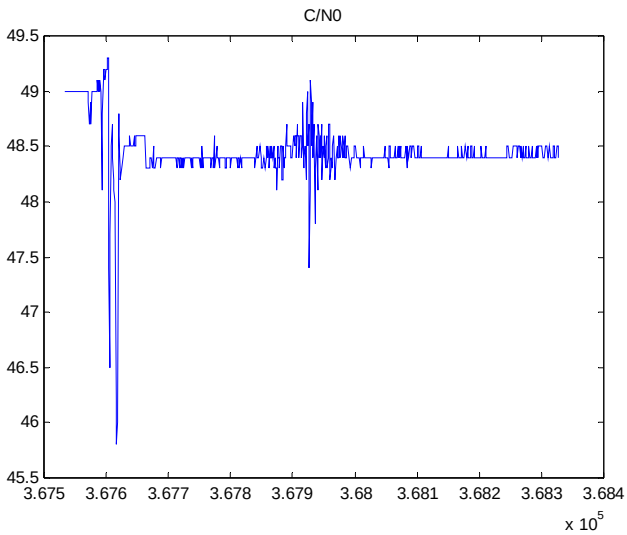

Figure 7: *Evolution of the C/N_0 as estimated by the receiver.*

As we can see on this graph, 250 seconds after the jammer has been powered on, the estimated C/N_0 starts to oscillate, its time evolution being constrained in a *sinc* envelope. That effect is clearly the illustration of the evolution of the correlation between the CW tone and the C/A code. Indeed, during the first 250 s, the cross-correlation is 0 because the jammer does not interact with any C/A code line. Then, as the received signal doppler shift nears 0, the correlator output is increasingly affected by the sine function resulting from the cross-correlation between the jammer and the targeted C/A code line.

The shape of the envelope of this sine function is determined by the *sinc* appearing in the expressions presented in section II. The argument of this *sinc* function is the frequency offset δf between the jammer and the targeted C/A code line, which is driven by the quasi-linear evolution of the doppler in this time interval.

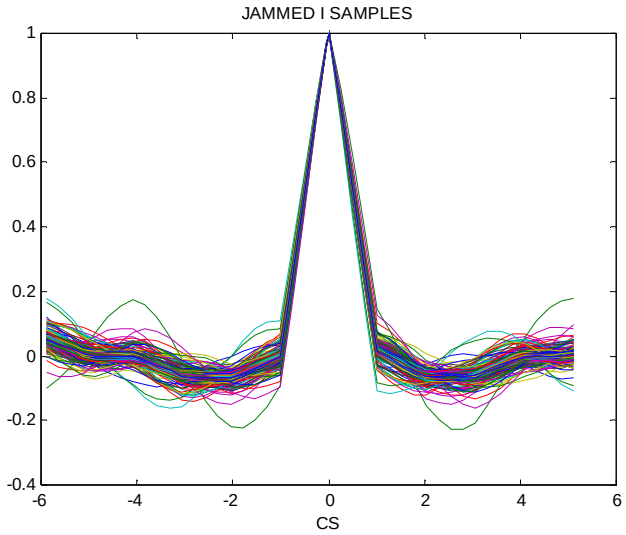

Figure 8: *Observed correlation peaks when jammer is on.*

Figure 8 shows the collection of the observed correlation peaks when the jammer is on. We can see that the correlator outputs are much more affected than in figure 6. In particular, the feet of the correlation triangle are now dominated by the sine function resulting from the cross-correlation between the jammer and the 227 kHz C/A code line.

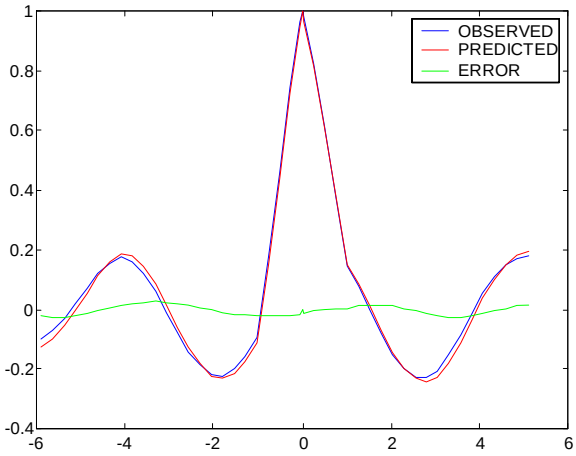

Figure 9: *Comparison of observed and predicted correlation function.*

As an example, figure 9 shows the output correlation function at the epoch where the amplitude of the sine function is maximum. We can clearly see that this function is the sum of the nominal triangle and the sine function. In this figure, the period of this sine function is 4.5 chips which corresponds to a frequency of 227 kHz. Figure 9 also shows the predicted value of this correlator output, which coincides perfectly well with the observed value, as shown by the plotted prediction error. This prediction was done using the expressions derived in section II. The amplitude of the sine function was computed from the power level values. The phase shift was computed using the observed Q channel samples.

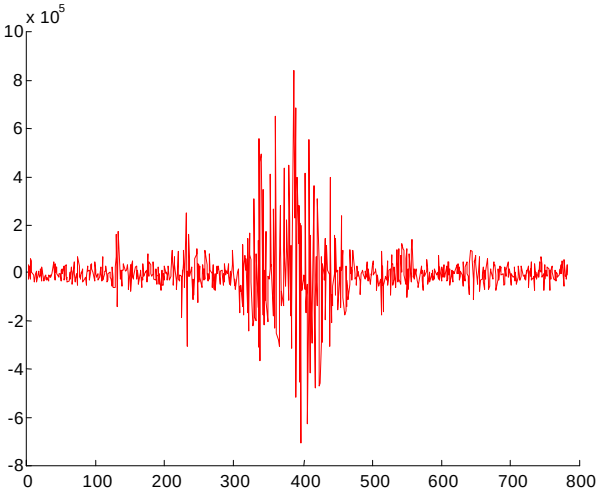

Figure 10: *Evolution of the output of one correlator (d=-4.6 chips from punctual).*

Figure 10 shows the evolution of one specific correlator output. We can see that this output is clearly affected by an oscillation that has a *sinc* envelope. As already discussed for figure 7, these oscillations are the result of the cross-correlation between the jammer tone and the targeted C/A code line. The envelope of these oscillations is the *sinc* function computed for the frequency offset between the jammer and the 227 kHz line. As the doppler of the received signal goes towards 0, we can clearly see the first two sidelobes of that *sinc* function, then the main lobe and then again the trailing two sidelobes. As the rate of evolution of the Doppler is 100 Hz per 200 s, we can see that the equivalent width of the main lobe is 100 Hz while the width of each sidelobe is 50 Hz. This is consistent with the expressions derived in section II.

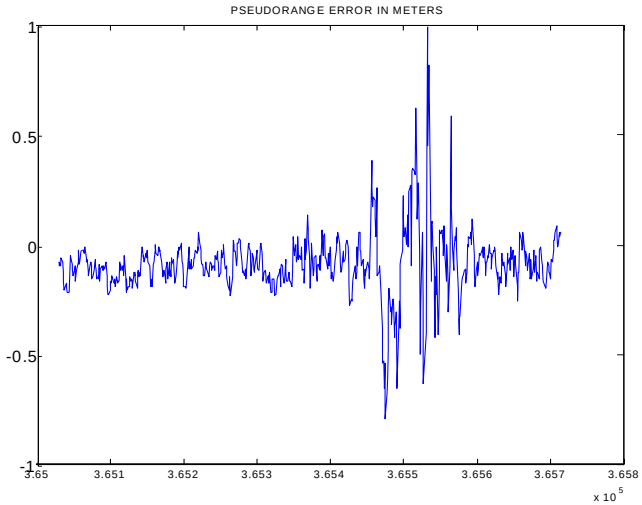

Figure 11: *Evolution of the code pseudorange error (J=-131 dBW).*

Figure 11 shows the evolution of the code pseudorange measurement error when the power of the jammer at the input of the receiver is –131 dBW. The maximum value of that error is observed when the correlation between the jammer and the 227 kHz line is maximum. At that point, the error is 1.13 m. The code-carrier smoothing filter time constant was set to 20 s for that test. Figure 12 shows again the observed pseudorange measurement error when the filter time constant is set to 10 s. This time, the maximum error is 2.71 m, which shows the increased resistance of the PLL with respect to the DLL.

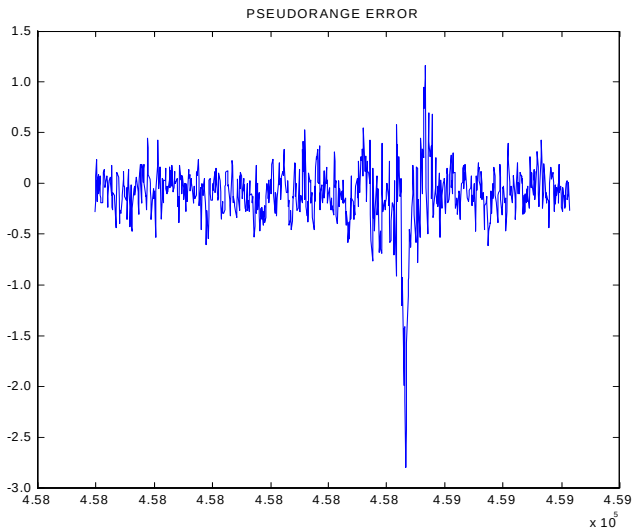

Figure 12: *Evolution of the code pseudorange error (J=-131 dBW) with a code-carrier smoothing filter time constant set to 10 s.*

Other tests were conducted with various frequencies and power levels. For example, a second test was run with a jammer hitting an average line at L1+209 kHz. That line has an individual power level of –30.7 dB with respect to the total C/A code power. Testing confirmed that correlator outputs did show a leakage of that line when Doppler was adequate, and that higher jammer powers were accepted by the tracking channel due to that lower value of the line weight.

During all the test series, the receiver tracking channel was sometimes seen tracking the jammer itself, the correlator output being dominated by the *sine* function itself. In these situations, the early minus late discrimination function is locked on the sine arch.

V. EFFECT OF FM INTERFERENCE

Another type of tests that were conducted aimed at analyzing the effect of larger band interference. The interference generator was then configured to generate a frequency modulated carrier. The modulation signal is simply a sine function. The carrier is set to be at L1+227 kHz.

For the first series of tests presented here, the single-sided bandwidth of the spectrum is 20 kHz. The total power of the FM signal is increased from -112 dB W to –109 dB W.

Figure 13 shows the evolution of the C/N_0 as computed by the receiver throughout that test. During the first minute after the jammer is turned on, the estimated C/N_0 oscillates between 51 dB Hz and -10 dB Hz, causing several losses of lock. After this transient period, the C/N_0 estimate drops by 15 dB and is stable over each input power interval. In this case, the C/N_0 estimate does not exhibit any additional oscillation produced by the perturbation of the correlator outputs.

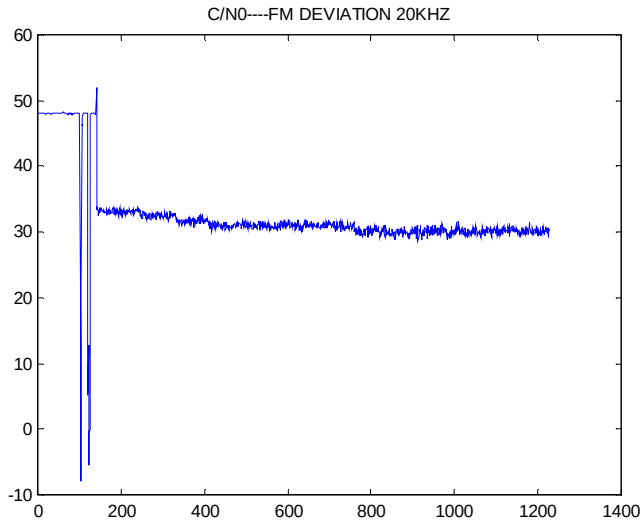

Figure 13: *Evolution of the C/N_0 as estimated by the receiver.*

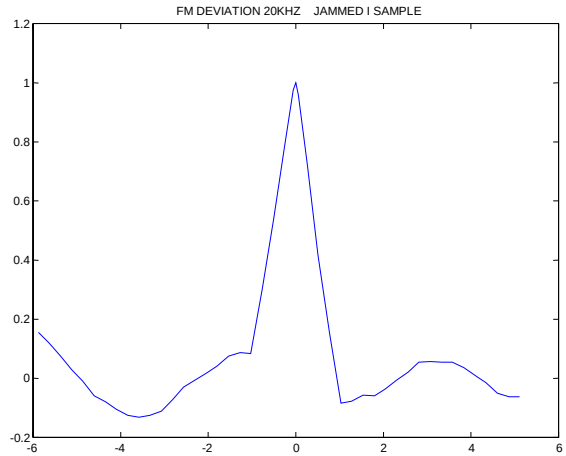

Figure 14: *Correlator output showing the result of the correlation between the FM signal and the C/A code.*

As an example, figure 14 shows the output correlation function at one particular epoch. As it appears in this figure, this function is dominated by the 227 kHz tone plus other oscillations. This function can be interpreted from the results presented in section II as the sum the cross-correlation between the sine functions composing the FM signal and the 40 targeted C/A code. As the amplitude of these correlation functions is determined by the power level of the C/A code hit line, the most powerful resulting function is the 227 kHz tone.

For the second series of tests presented, the single sided bandwidth of the FM spectrum is set to 100 kHz. The power level of the FM signal at the output of the signal generator is increased from -113 dB W to -111 dB W and finally -108 dB W.

Figure 15 shows the evolution of the C/N0 as computed by the receiver throughout that test The estimated C/N_0 estimate drops immediately by 15 dB and is stable over each input power interval. In this case, the C/N_0 estimate does not exhibit any additional oscillation produced by the perturbation of the correlator outputs.

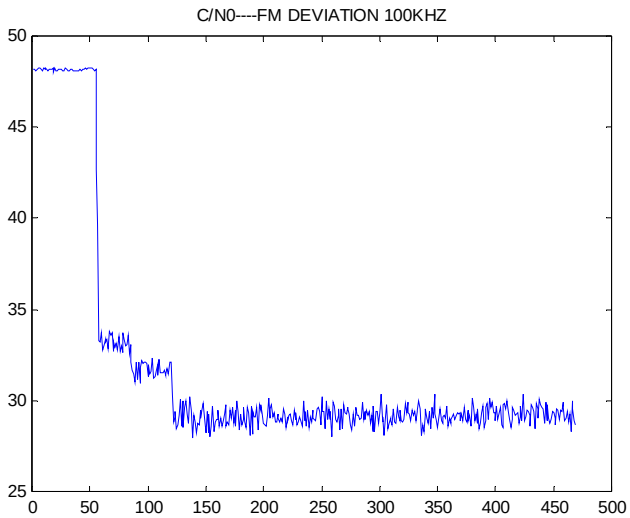

Figure 15: *Evolution of the C/N_0 as estimated by the receiver.*

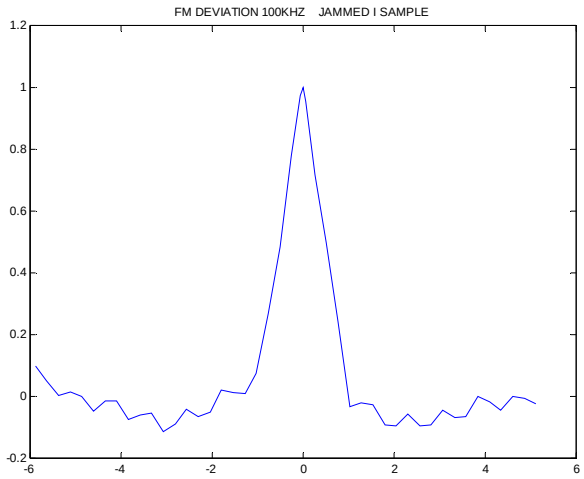

Figure 16: *Correlator output showing the result of the correlation between the FM signal and the C/A code.*

As an example, figure 16 shows the output correlation function at one particular epoch. As it appears in this figure, this function is affected by several oscillations and the 227 kHz tone is no longer the dominant result, as 200 C/A code lines are impacted.

The observed pseudorange tracking error is limited to 0.95 m when the interfering signal is the 20 kHz FM and to 1.04 m when the interfering signal is the 100 kHz FM.

VI EFFECT ON POSITION SOLUTION

In order to test for the behaviour of the complete multi-channel receiver in presence of CW interference, we re-configured the receiver into a 12-channel L1 GPS receiver and recorded the output range measurements and position status.

The results presented here were obtained by injecting a CW at L1+1 kHz with a power level of –111 dB W. The RF signal was set on at 364000 s within the scenario.

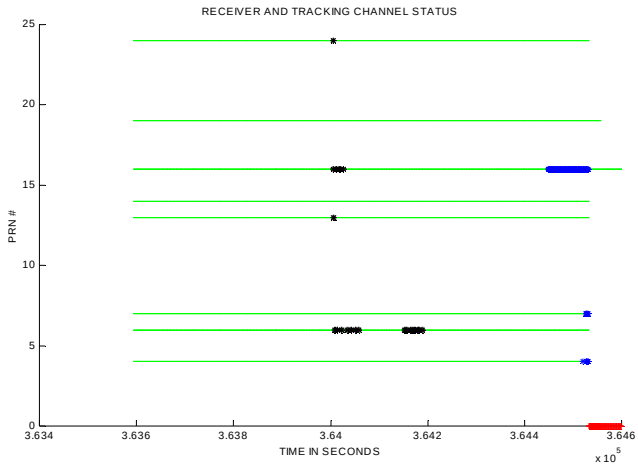

Figure 17: *Evolution of receiver and channel tracking status over time.*

Figure 17 shows the evolution of the status of the channels tracking each of the 8 indicated satellites over time. In addition, it shows the evolution of the position solution status on the bottom line. The green dots indicate that the range measurement is valid and is being used in the position solution. The black stars indicate that the estimated C/N_0 in the channel has dropped below the acceptable tracking threshold. The blue stars indicate a misclosure due to an excessive gap between the estimated and the actual positions. The red stars indicate that the position solution is not valid because a test distance is exceeded.

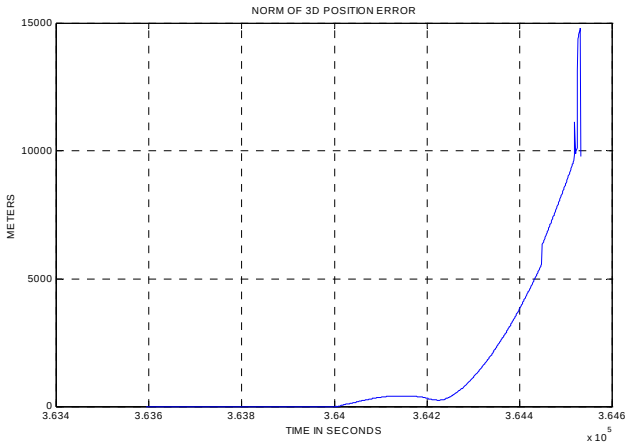

Figure 18: *Evolution of position solution error over time.*

Figure 18 shows the evolution of the position solution error over time. As we can seen, the position error start to slowly increase immediately after the jammer has been switched on to reach a few hundreds of meters. Then, 220 s after the jammer is on, the error increases rapidly to reach 15 km 470 s later. A few seconds after that extreme value is reached, the position solution is declared invalid.

Figure 19 shows the evolution of the detected doppler shift of the signal tracked in the channel initially tracking PRN 6. As we can see, the doppler has a nominal evolution before the jammer is on, and then this evolution is disrupted, jumps are visible, then the Doppler evolution departs from the original trend. This can be explained by the fact that the receiver no longer tracks the GPS signal but rather the jammer. This is also visible in figure 20 showing the evolution of the estimated C/N_0 in that tracking channel. As we can see, the C/N_0 oscillates and finally drops by 12 dB after the jammer is switched on, then the value stays low at 34 dB Hz for 100 s, then that value drops again to a very low value this time and finally stays up at 34 dB Hz.

Observation of these quantities for all the tracking channels shows that all of them are fooled by the jammer. Therefore the position solution is being driven away by the interferer and the receiver only detects that drift when the position error is of the order of several km.

Testing with a GPS receiver equipped with a RAIM configured for NPA showed that the resistance of that receiver is greatly improved with such a feature. In that case, the receiver detects very quickly the inconsistency of some of the range measurements and either rejects the solution as a whole or excludes one of the measurements.

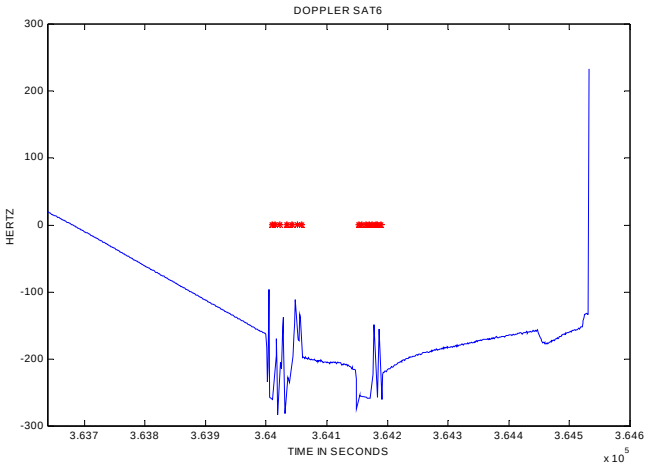

Figure 19: *Evolution of doppler shift of tracked signal in the channel initially tracking PRN .*

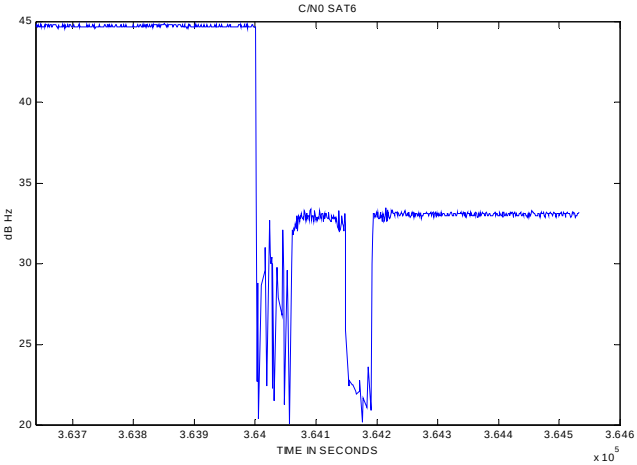

Figure 20: *Evolution of estimated C/N_0 in the channel initially tracking PRN .*

VII CONCLUSION

The theoretical developments presented in the second section show the impact of a CW jammer on the correlator outputs. The predicted amplitude of the induced perturbation depends on the relative amplitude of the jammer and the received GPS signal, on the frequency offset between the jammer and the nearest C/A code line and on the weight of that spectrum line.

Observations of the correlator outputs using a multicorrelator receiver confirmed these results in several test cases involving CW jamming at different frequencies and power levels.

When the receiver is not tracking the jammer, the induced pseudorange measurement errors have a modest amplitude of a few meters depending on the code-carrier filter smoothing time constant.

Additional tests show that the CW analysis could be extended to FM jammers.

Testing with a multichannel receiver enabled to analyze the behaviour of the position solution. It was shown that in a very simple configuration (CW jammer at L1+1kHz, receiver input power level –111 dBW), many tracking channels may simultaneously be affected leading to tremendous position errors in the absence of RAIM.

Future work will focus on the development of techniques allowing detection and identification of several types of jammers.

ACKNOWLEDGMENTS

This study was made possible through the joint funding of STNA and the European Commission in the frame of TEN/99/179 project for Pre-Operational Data Gathering to Support Multi-Modal SBAS Certification.

REFERENCES

[Bastide et Julien, 2000] F. BASTIDE and O. JULIEN " Effects of Interference and Multipath on GPS signals "

[Betz, 2000], J. BETZ, "Effect of Narrowband Interference on GPS Code Tracking Accuracy", proceedings of ION NTM 2000.

[Bye et al., 1998], C. BYE, G. HARTMANN and A. KILLEN, "Development of a FOG-Based GPS-INS", IEEE PLANS 98.

[Julien, 2000] O. JULIEN, " Effects of Interference on GPS signals "

[Przyjemski et al., 1993], J. PRZYJEMSKI, J. BALBONI, E. DOWDLE and B. HOLSAPPLE, "GPS Anti-Jam Techniques", proceeding of ION GPS-93

[Spilker and Natali, 1996], J. SPILKER and F. NATALI, "Interference Effects and Mitigation Techniques", Chapter 20 of 'Global Positioning System: Theory and Applications', AIAA.

[Ward, 1996], P. WARD, "Effects of RF Interference on GPS Satellite Signal Receiver Tracking", Chapter 6 of 'Understanding GPS: Principles and Applications', E. Kaplan Editor, Artech House